

# Chemical Science

Accepted Manuscript



This article can be cited before page numbers have been issued, to do this please use: S. Pellegrino, N. Tonali, E. Erba, J. Kaffy, M. Taverna, A. Contini, M. Taylor, D. Allsop, M. L. Gelmi and S. Ongerì, *Chem. Sci.*, 2016, DOI: 10.1039/C6SC03176E.



This is an *Accepted Manuscript*, which has been through the Royal Society of Chemistry peer review process and has been accepted for publication.

*Accepted Manuscripts* are published online shortly after acceptance, before technical editing, formatting and proof reading. Using this free service, authors can make their results available to the community, in citable form, before we publish the edited article. We will replace this *Accepted Manuscript* with the edited and formatted *Advance Article* as soon as it is available.

You can find more information about *Accepted Manuscripts* in the [Information for Authors](#).

Please note that technical editing may introduce minor changes to the text and/or graphics, which may alter content. The journal's standard [Terms & Conditions](#) and the [Ethical guidelines](#) still apply. In no event shall the Royal Society of Chemistry be held responsible for any errors or omissions in this *Accepted Manuscript* or any consequences arising from the use of any information it contains.

## $\beta$ -Hairpin mimics containing a piperidine-pyrrolidine scaffold modulate the $\beta$ -amyloid aggregation process preserving the monomer species

S. Pellegrino<sup>a\*</sup>, N. Tonali<sup>b</sup>, E. Erba<sup>a</sup>, J. Kaffy<sup>b</sup>, M. Taverna<sup>c</sup>, A. Contini<sup>a</sup>, M. Taylor<sup>d</sup>, D. Allsop<sup>d</sup>, M. L. Gelmi<sup>a</sup> and S. Ongerib<sup>b\*</sup>

Received 00th January 20xx,  
Accepted 00th January 20xx

DOI: 10.1039/x0xx00000x

www.rsc.org/

Alzheimer's disease is a neurodegenerative disorder linked to oligomerization and fibrillization of amyloid  $\beta$  peptides, with  $A\beta_{1-42}$  being the most aggregative and neurotoxic one. We report herein the synthesis and conformational analysis of  $A\beta_{1-42}$ -amyloid related  $\beta$ -hairpin peptidomimetics, built on a piperidine-pyrrolidine semi rigid  $\beta$ -turn inducer and bearing two small recognition peptide sequences, designed on oligomeric and fibril structures of  $A\beta_{1-42}$ . According to these peptide sequences, a stable  $\beta$ -hairpin or a dynamic equilibrium between two possible architectures was observed. These original constructs are able to greatly delay the kinetics of  $A\beta_{1-42}$  aggregation process as demonstrated by thioflavin-T fluorescence, and transmission electron microscopy. Capillary electrophoresis indicates their ability to preserve the monomer species, inhibiting the formation of toxic oligomers. Furthermore, compounds protect against toxic effects of  $A\beta$  on neuroblastoma cells even at substoichiometric concentrations. This study is the first example of acyclic small  $\beta$ -hairpin mimics possessing such a highly efficient anti-aggregation activity. The protective effect is more pronounced than that observed with molecules which have undergone clinical trials. The structural elements made in this study provide valuable insights in the understanding of the aggregation process and insights to explore the design of novel acyclic  $\beta$ -hairpin targeting other types of amyloid-forming proteins.

### Introduction

Amyloid fibrils are self-assembled insoluble aggregates characterized by highly ordered cross- $\beta$  structures. They constitute the hallmark of more than 20 serious human amyloidosis diseases, such as Alzheimer's disease (AD), Parkinson's neurodegeneration, type II diabetes and spongiform encephalopathy.<sup>1</sup> In particular, AD is associated with the aggregation of the amyloid- $\beta$  ( $A\beta_{1-42}$ ) peptide into senile plaques in the brain.<sup>2</sup> A large number of small molecules have been proposed for their ability to inhibit or modulate  $A\beta_{1-42}$  aggregation and toxicity. However, the aggregation process is highly complex, and extremely difficult to control.<sup>3</sup> Fibrils are able to generate damaging redox activity and promote the nucleation of toxic oligomers.<sup>4</sup> Recent studies indicate that soluble transient oligomers preceding fibril formation are highly toxic species.<sup>5</sup> Their

characterization and the activity of  $A\beta_{1-42}$  aggregation inhibitors on these small and toxic oligomeric species is generally lacking. Thus, the development of inhibitors targeting both oligomerization and fibrillization remains challenging despite its therapeutic significance.<sup>4c</sup>

Peptides are today reasonable alternatives to small molecule pharmaceuticals. They often offer greater efficacy, selectivity, specificity and a reduced risk of unforeseen side-reactions compared to small organic molecules, while some of their pharmacodynamic weaknesses can be circumvented by innovative formulations.<sup>6</sup> A variety of small peptides that inhibit aggregation of  $A\beta$  and reduce its toxic effects have been already described.<sup>7</sup> In particular, inhibition of  $A\beta$ -aggregation has been targeted using self-recognition elements (SREs). Indeed, molecules based on fragments of the  $A\beta$ -peptide, essentially on the nucleation sequence  $A\beta_{16-20}$  (KLVFF), were found promising as SREs.<sup>8</sup> The design of macrocycles  $\beta$ -sheet mimics containing an unnatural tripeptide unit (Nowick's Hao) and SREs, has been a valid strategy.<sup>9</sup> To our knowledge, the use of small acyclic  $\beta$ -hairpins has been very rarely explored as  $\beta$ -sheet binders and inhibitors of aggregation.<sup>10</sup>

Interestingly, compounds possessing several kinetically and thermodynamically accessible local minima representing conformations might be much more powerful inhibitors with respect to rigid ones in modulating protein-protein interactions.<sup>11</sup> As  $A\beta$ -aggregation is a dynamic and complex process, we hypothesized that flexible  $\beta$ -hairpins could adapt themselves in the interaction with the different  $A\beta_{1-42}$  conformations present during the aggregation process, and in particular in the early stages of

<sup>a</sup> DISFARM-Sez. Chimica Generale e Organica "A. Marchesini", Università degli Studi di Milano, via Venezian 21, 20133 Milano, Italy. sara.pellegrino@unimi.it

<sup>b</sup> Molécules Fluorées et Chimie Médicinale, BioCIS, Univ. Paris-Sud, CNRS, Université Paris Saclay, 5 rue Jean-Baptiste Clément, 92296 Châtenay-Malabry Cedex, France.

<sup>c</sup> Protéines et Nanotechnologies en Sciences Séparatives, Institut Gallien Paris-Sud, Univ. Paris-Sud, CNRS, Université Paris Saclay, 5 rue Jean-Baptiste Clément, 92296 Châtenay-Malabry Cedex, France. Sandrine.ongerib@u-psud.fr

<sup>d</sup> Lancaster University, Division of Biomedical and Life Sciences, Faculty of Health and Medicine, Lancaster LA1 4YQ, UK.

Electronic Supplementary Information (ESI) available: [Computational methods and additional figures and tables. NMR additional data. Description of synthetic procedures and characterization of compounds. Experimental procedure for fluorescence-detected ThT binding assay; representative curves of ThT fluorescence assays. Experimental procedure for TEM studies, CE, and cellular evaluation]. See DOI: 10.1039/x0xx00000x



oligomerization. For that purpose, we designed two acyclic,  $\beta$ -hairpin mimics **G1** and **G2** based on the piperidine-pyrrolidine semi-rigid scaffold **S1**,<sup>12</sup> developed recently as a flexible  $\beta$ -turn inducer (Figure 1), and on different SREs of A $\beta$ <sub>1-42</sub>. The nucleation sequence A $\beta$ <sub>16-20</sub> (KLVFF) has been introduced in the C-terminal sequence of both **G1** and **G2**. However, the choice of the N-terminal sequence was driven by the strategy to develop both a flexible and a more structured  $\beta$ -hairpin. The hydrophobic sequence G<sub>33</sub>LMVG<sub>37</sub>, facing K<sub>16</sub>LVFF<sub>20</sub> in the more flexible oligomeric structures<sup>13</sup> has been introduced in **G1**. In **G2**, GVVIE has been chosen as a mimic of the hydrophobic sequence G<sub>38</sub>VVIA<sub>42</sub>, facing K<sub>16</sub>LVFF<sub>20</sub> in the stable fibril structures.<sup>14</sup> The alanine residue has been replaced by glutamic acid in order to possibly engage an ionic interaction with the facing lysine residue, thus stabilizing the  $\beta$ -hairpin structure (Figure 1). The N-terminal amino acid of both **G1** and **G2** was either acetylated (**G1a**, **G2a**) or not (**G1b**, **G2b**), in order to evaluate the capacity of the compounds to engage electrostatic interactions with acidic residues of A $\beta$ <sub>1-42</sub> and with the view to increase their affinity. Several computational and experimental studies on A $\beta$ <sub>1-42</sub> proved in fact that, in addition to the hydrophobic interactions involving in particular the 16-21 sequence (KLVFFA), the formation of a salt-bridge between amino acids Asp23 and Lys28 of amyloid might stabilize a turn motif involving residues 24-28.<sup>13</sup> An interaction with Glu22 might be also promoted and beneficial for the activity of the molecules.<sup>15</sup>

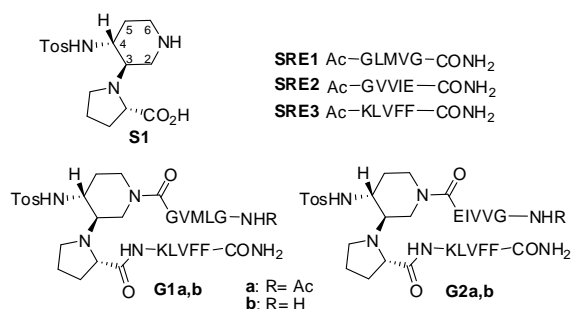


**Figure 1.** Structure of  $\beta$ -amyloid mimics **G1** and **G2** and the corresponding SREs

## Results and discussion

**Conformational studies and synthesis.** In order to evaluate the folding propensity of the designed **G1** and **G2**  $\beta$ -hairpin mimics, as well as to get preliminary information on their conformational stability, we performed a computational study using replica exchange molecular dynamics (REMD) on **G1a** and **G2a**.<sup>16,17,18</sup> Thus, we simulated peptides **G1a** and **G2a** using the *ff96* force field coupled with the OBC(II) solvent model,<sup>19</sup> (see Supporting Information (SI) for additional details). The secondary structure analysis by DSSP<sup>20</sup> (Tables S1 and S2, SI) showed that both peptides have a relatively high tendency to form anti-parallel  $\beta$ -sheets. **G2a** seemed to form a very stable  $\beta$ -hairpin, with percentage values of anti-parallel  $\beta$ -sheet content, relatively to non-terminal amino acids, ranging from about 60 to about 90%. **G1a** was somehow less stable, with an anti-parallel  $\beta$ -sheet content averagely 20% less than **G2a**. In the H-bond analyses (Tables S3 and S4, SI) two pairs of very

stable H-bonds, involving the backbone NH and C=O atoms of residues Ile4/Leu8 and Val2/Phe10, were observed for **G2a**. On the other hand, the occupancies of intramolecular H-bonds detected for **G1a** were lower. We observed a minor populated hairpin conformation, characterized by the H-bonds involving Val4/Leu8 and Leu2/Phe10, and a major "mismatched" hairpin involving Val4/Val9 and Leu2/Phe11. The representative structures of the most populated cluster for **G1a** and **G2a** (Figure 2) showed a mismatched  $\beta$ -hairpin for the former peptide, with the N-terminal strand (Gly1-Gly5) that was shifted one residue with respect to the C-terminal strand (Lys7-Phe11). Conversely, for **G2a**, the two strands were perfectly matched. The higher conformational flexibility of **G1a**, compared to **G2a**, was also shown by the root mean square deviation (RMSD) analysis of the corresponding REMD trajectories (Figure S1, SI), confirming the possibility of an equilibrium for the former peptide between multiple  $\beta$ -hairpin like conformations, while a single and fairly rigid  $\beta$ -hairpin conformation was predicted for **G2a**.

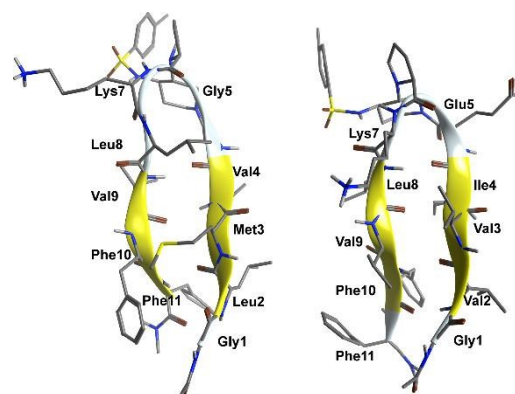


**Figure 2.** Representative structures of the most populated cluster obtained from cluster analyses of the 302.76 K trajectory of REMD simulations for peptides **G1a** (left) and **G2a** (right).

Compounds **G1** and **G2** were thus prepared by solid phase peptide synthesis, using the Fmoc strategy (see SI for details).<sup>21</sup> In order to evaluate the efficacy of **G1** and **G2** molecules with respect to a truncated derivative or the single arms, we also prepared derivative **G3** (Figure 3), containing the scaffold and only the A $\beta$ (16-20) SRE, and compounds **SRE1-3** corresponding to the different SREs (Figure 1, see SI for details).

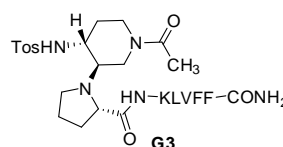


**Figure 3.** Structure of truncated mimic **G3**

The CD spectra of **G1a** and **G2a** were recorded in MeOH at 25 °C (Figure 4). **G1a** showed a negative band at 195 nm indicating that in solution this peptidomimetic did not assume a preferred, single conformation. On the other hand, the spectrum of **G2a** was characterized by a strong positive Cotton



effect at around 195 nm ( $\pi$ - $\pi^*$  energetic transition), and a negative band at around 215 nm ( $n$ - $\pi^*$  energetic transition), typical of  $\beta$ -sheet structures.

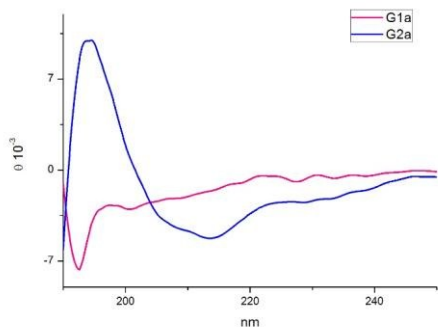


**Figure 4.** CD spectra of compounds **G1a** and **G2a** in MeOH

The different behaviour of **G1a** and **G2a** was confirmed by  $^1\text{H-NMR}$  experiments in  $\text{CD}_3\text{OH}$  (Tables S6-S8 in SI). Compound **G1a** is present in solution as two different  $\beta$ -hairpin structures (**G1a-1**/**G1a-2**, 2:1 ratio, Figure 5), characterized by a different alignment of the two peptide arms. This dynamic equilibrium is proved by the presence of several negative NH/NH ROEs (Figure S4, SI).<sup>22</sup> On the other hand,  $^1\text{H}$  NMR spectrum of **G2a** showed a good dispersion of the NH chemical shifts indicating the presence of a stable single  $\beta$ -hairpin conformation characterized by a peptide arms alignment similar to **G1a-2** (Figure 5 on the bottom).<sup>23</sup>

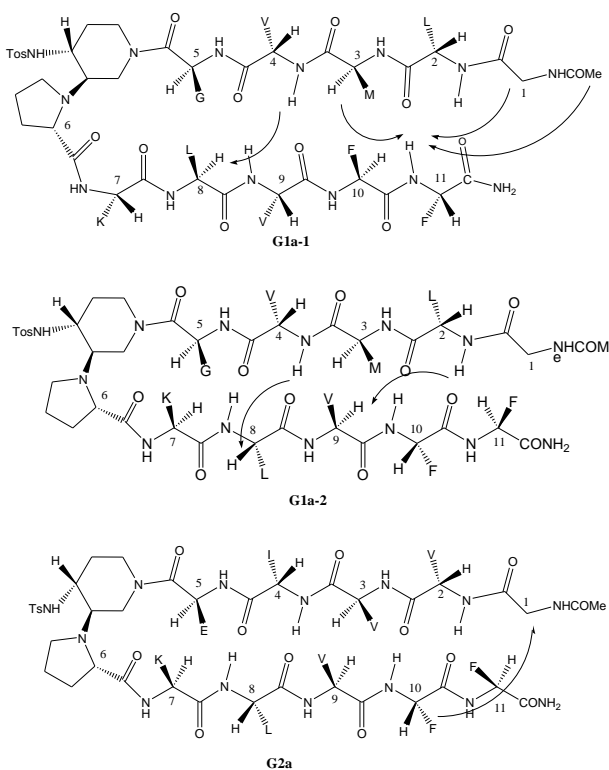


**Figure 5.**  $\beta$ -Hairpin structures of compounds **G1a-1**, **G1a-2**, and **G2a**, showing the assigned ROEs

ROESY experiments confirmed the presence of a turn structure in **G1a-1**, **G1a-2**, and **G2a**, as already reported for model sequences (Figure S5 and Figure S11, SI).<sup>12a</sup>

Several sequential  $\text{CH}\alpha/\text{NH}$  ROEs, indicating  $\beta$ -conformations, were found for both **G1a-1** and **G1a-2** isomers (Figures 5 and S6, SI). The different alignment of the peptide chains was proven by a ROE between  $\text{NH}_{\text{Phe11}}/\text{CH}\alpha_{\text{Met3}}$  in **G1a-1**, and by another one between  $\text{NH}_{\text{Leu2}}/\text{CH}\alpha_{\text{Val9}}$  in **G1a-2** (for a complete discussion see SI). Regarding compound **G2a** we could detect only one  $\beta$ -hairpin diagnostic ROE between  $\text{CH}\alpha_{\text{Gly1}}$  and the phenyl ring of Phe-10 (Figures 5 and S12, SI). Several  $\text{CH}\alpha$  signals are indeed overlapped or masked by the solvent. The presence of a  $\beta$ -hairpin structure was confirmed by  $^3\text{J}_{\text{HN/CH}\alpha}$  coupling constants that are higher than 8 Hz (Table TS9, SI).<sup>24,25</sup>

Finally, the  $\beta$ -hairpin conformation was definitively confirmed for all compounds by the positive difference between experimental  $\text{H}\alpha$  chemical shift values and "random" ones<sup>26</sup> (Figure 6). Only Met-3 of **G1a-1** is characterized by a negative  $\Delta\delta\alpha\text{H}$  value. This is probably due to the anisotropic effect<sup>27</sup> of the aromatic ring of Phe-11 that faces Met-3, as evicted from ROESY experiments (Figure S6A, SI).

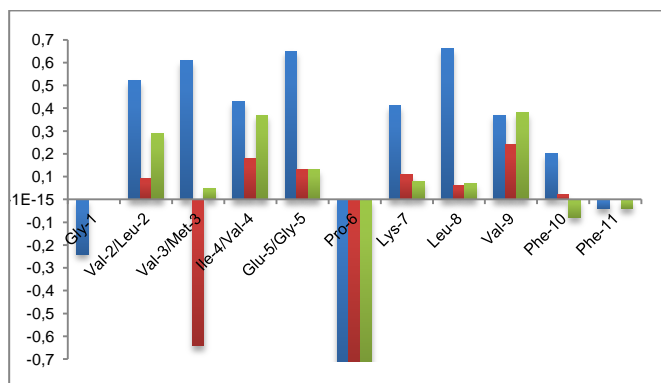


**Figure 6.** NMR analysis. Plot of difference between  $\text{H}\alpha$  chemical shift values in the random coil and the values determined experimentally for **G2a** (blue) and isomers **G1a-1** (red) and **G1a-2** (green) in  $\text{CD}_3\text{OH}$  at 298 K.

Taking together both experimental and theoretical results, we can conclude that different hairpin architectures are possible for **G1a** and **G2a**, depending on the *N*-terminus sequence. The GVVIE motif in **G2a** strongly stabilizes a single "matched" hairpin conformation. On the other hand, the GLMVG motif in **G1a** gave a dynamic equilibrium between two possible architectures, the "mismatched" hairpin being the more stable.

**Inhibition of  $\text{A}\beta_{1-42}$  fibrillization.** The ability of compounds **G1-3** and **SRE1-3** to interact with  $\text{A}\beta_{1-42}$  during the fibrillation process was first studied by Thioflavin-T (ThT) fluorescence spectroscopy.<sup>28</sup> The fluorescence curve for  $\text{A}\beta_{1-42}$  at a concentration of 10  $\mu\text{M}$  followed the typical sigmoid pattern with a lag phase of 4-5 h followed by an elongation phase and a final plateau reached after 10-12 h (Figure 7a). Two parameters were derived from the ThT curves of  $\text{A}\beta_{1-42}$





alone and in the presence of the evaluated compound: (1)  $t_{1/2}$ , is defined as the time at which the half maximal ThT fluorescence is observed, which gives insight on the rate of the aggregation process; (2) the fluorescence intensity at the plateau (F) which is assumed to depend on the amount of fibrillar material formed (Table 1).

Both **G1** and **G2** series are able to inhibit  $A\beta_{1-42}$  aggregation. The **G1** series, containing the sequence  $G_{37}VMLG_{33}$ , and possessing a dynamic equilibrium between two different  $\beta$ -hairpin conformations, exerts a slightly superior inhibitory activity (Figure 7 and Table 1). Furthermore, the free terminal amine is also important for  $A\beta_{1-42}$  aggregation suppression. Unprotected **G1b** and **G2b** were indeed able to totally suppress aggregation at compound/ $A\beta_{1-42}$  ratio of 10/1 and still dramatically delayed  $A\beta_{1-42}$  aggregation at 1/1 ratio (Figure 7a) and Table 1). Acetylated derivatives **G1a** and **G2a** retained this activity, but to a lesser extent (Table 1 and Figure S14). This result supports our hypothesis on the importance of establishing an ionic interaction between the *N*-terminal amino group and acidic residues of  $A\beta_{1-42}$ .

No activity was observed for the isolated pentapeptides GLMVG (**SRE1**) and GVVIE (**SRE2**) (Table S11 and Figure S14). KLVFF (**SRE3**) delayed  $A\beta_{1-42}$  aggregation at compound/ $A\beta_{1-42}$  ratio of 10/1,<sup>8a,29</sup> however in a much lesser extent than **G1** and **G2** series, while exerted no activity at 1/1 ratio (Table S11). The **G3** intermediate containing KLVFF linked to the piperidine-pyrrolidine scaffold **S1** is more active than **SRE3**. These results highlight that the piperidine-pyrrolidine scaffold **S1** and the pentapeptide KLVFF are both crucial for the activity, but the whole  $\beta$ -hairpin construct is necessary to strongly delay the  $A\beta_{1-42}$  aggregation kinetics.

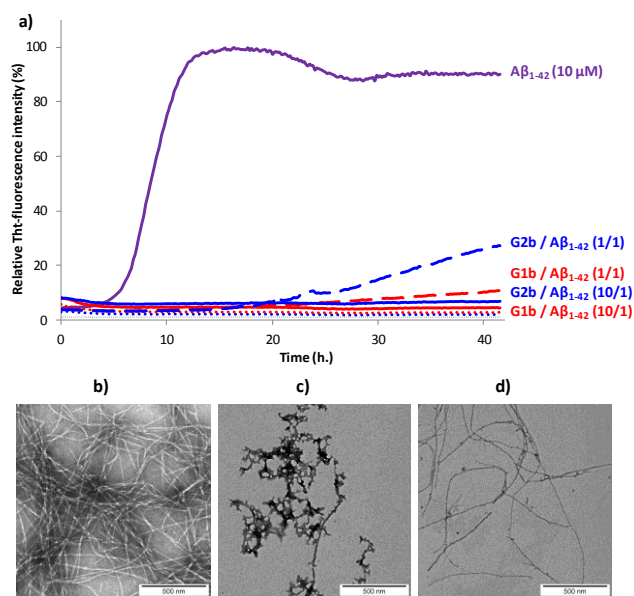


**Figure 7.** a) Representative curves of ThT fluorescence assays over time showing  $A\beta_{1-42}$  (10  $\mu$ M) aggregation in the absence (purple curve) and in the presence of compounds **G1b** (red curves) and **G2b** (blue curves) at compound/ $A\beta_{1-42}$  ratios of 10/1 and 1/1. The control curves are represented in dotted lines (**G1b** in red, **G2b** in blue and grey for buffer). Fibril formation of  $A\beta_{1-42}$  visualized by TEM: negatively stained images recorded after 42 h of incubation of  $A\beta_{1-42}$  (10  $\mu$ M in 10 mM Tris.HCl, 100 mM NaCl at pH = 7.4) alone (b)

or in the presence of 10  $\mu$ M of **G1b** (c) or **G2b** (d). Scale bars represent 500 nm.

DOI: 10.1039/C6SC03176E

**Table 1.** Effects of compounds **G1-2** on  $A\beta_{1-42}$  fibrillization assessed by ThT-fluorescence spectroscopy at 10/1 and 1/1 compound/ $A\beta$  ratios (the concentration of  $A\beta_{1-42}$  is 10  $\mu$ M) and compared to the values obtained for  $A\beta_{1-42}$  alone ( $t_{1/2}$  and F).

Compounds (Compound/ $A\beta$ ratio)	$t_{1/2}$ extension <sup>[a]</sup>	Change of fluorescence intensity at the plateau (%) <sup>[b]</sup>
<b>G1a</b> (10/1)	NA	-97±1%
<b>G1a</b> (1/1)	2.06±0.12	-71±2%
<b>G2a</b> (10/1)	Sat [c]	Sat [c]
<b>G2a</b> (1/1)	1.76±0.11	-41±7%
<b>G1b</b> (10/1)	NA	-97±1%
<b>G1b</b> (1/1)	NA	-90±2%
<b>G2b</b> (10/1)	NA	-95±1%
<b>G2b</b> (1/1)	>3.56±0.12	-73±3%

NA = no aggregation, parameters are expressed as mean  $\pm$  SE, n=3-6. [a] See SI for the calculation of the  $t_{1/2}$  extension. A compound displaying a  $t_{1/2}$  increase > 1 is a delayer of aggregation. [b] See SI for the calculation of the change of fluorescence intensity at the plateau. [c] Sat means that a saturation of the fluorescence signal is observed because **G2a** self-aggregates at 100  $\mu$ M.

In order to assess the selectivity on  $A\beta_{1-42}$  peptide, the ability of compounds **G1b** and **G2b** to interact with IAPP (islet amyloid polypeptide), an amyloid protein involved in type 2 diabetes mellitus but having another SRE,<sup>30</sup> was also tested by the ThT-fluorescence assay under conditions similar to that described for  $A\beta_{1-42}$  peptide. It is noteworthy that both compounds displayed no activity on IAPP fibrillization process at compound/ $A\beta_{1-42}$  ratio of 1/1 and only slightly delayed it at the higher ratio (10/1) (Figure S15). This result suggests that the inhibition of aggregation displayed by compounds **G1b** and **G2b** on  $A\beta_{1-42}$  peptide is sequence specific.

Transmission electron microscopy (TEM) analyses were performed on the most promising **G1a**, **G1b** and **G2b** compounds. Images were recorded at 20 h and 42 h of fibrillization kinetics with samples containing 10  $\mu$ M of each compound corresponding to the compound/ $A\beta_{1-42}$  ratio of 1/1 (Figures 7b-d) and S16). Differences were observed in both quantity and morphology of aggregates formed. At 42 h, a very dense network of fibers displaying a typical morphology was observed for  $A\beta_{1-42}$  alone (Figure 7b). In the samples containing **G1a**, the network of fibers was significantly less dense than in the control experiment after 20 h and 42 h. However, the fibers displayed the same morphology (Figure S16, SI). In the samples containing **G2b**, the same trends as with **G1a** were observed (Figures 7d and S16). In samples containing **G1b**, we mainly observed globular aggregates after 20 h and 42 h (Figures 7c) and S16) indicating that the aggregation pathway could be



different from the one observed for  $A\beta_{1-42}$  alone. These results validated the ThT-fluorescence data, indicating that compounds **G1a**, **G1b** and **G2b** dramatically slowed down the aggregation of  $A\beta_{1-42}$  and efficiently reduced the amount of typical amyloid fibrils.

**Inhibition of  $A\beta_{1-42}$  oligomerization.** Compounds **G1b** and **G2b** were finally studied (at compound/ $A\beta_{1-42}$  ratio of 1/1) by Capillary Electrophoresis (CE) using a method we recently proposed to monitor the very early steps of the oligomerization process overtime and to analyze the effect of drugs on these challenging first stages.<sup>31</sup> We focused our attention on three kinds of species: (1) the monomer (peak ES), (2) different small metastable oligomers grouped under peak ES' and (3) transient species formed later and which correspond to species larger than dodecamers but still soluble (peak LS). Aggregation kinetics of  $A\beta_{1-42}$  peptide alone (Figures 8a and S18) showed that overtime, the monomer ES peak decreased in favor of the oligomer peaks ES' and LS, and that insoluble species, forming spikes in the profile, appeared after 8 hours.

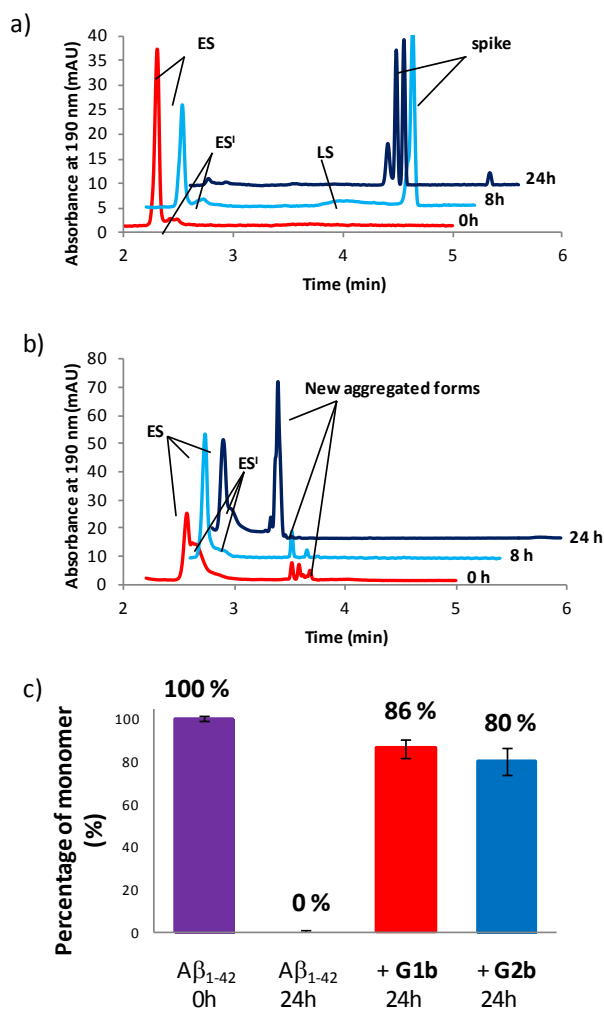


**Figure 8.** Electrophoretic profile obtained immediately (0 h, red), 8 h (blue) and 24 h (purple) after sample dissolution of  $A\beta_{1-42}$  peptide (100  $\mu$ M) a) alone or b) in the presence of **G1b**

(100  $\mu$ M). c) Peak area of the monomer (ES) related to its peak area in the sample of  $A\beta_{1-42}$  alone at 0h. DOI: 10.1039/C6SC03176E

In the presence of **G1b**, the aggregation kinetics of  $A\beta_{1-42}$  peptide was greatly modified (Figures 8b and S19). Noteworthy, the monomeric species (peak ES) was dramatically stabilized. 86% of the monomer remained after 24 h in the presence of **G1b**, while it was no more detected in the control sample (Figure 8c). Moreover, the larger aggregated species LS (> dodecamers) were not detected. New aggregated forms of  $A\beta_{1-42}$ , between ES' and LS migration times were observed on each electrophoretic profile. We checked that these new aggregated forms were not due to **G1b** degradation or self-assemblies (Figure S17A.) They were probably aggregated forms with a different morphology than both LS and those giving spikes observed in  $A\beta_{1-42}$  control. This observation is in accordance with the TEM images where globular aggregates were observed instead of the classical dense network of fibers (Figures 7c and S16). In ThT-assays, no fluorescence was detected, indicating that the globular species were not characterized by highly ordered  $\beta$ -structures (Figure 7a). Remarkably, the presence of the monomer was maintained even after 4 days (Figure S19B). We concluded that **G1b** is able to prevent the formation of toxic soluble oligomers of  $A\beta_{1-42}$  peptide and to maintain the presence of the non toxic monomer overtime.

**G2b** also dramatically maintained the presence of the monomer (peak ES, 80% after 24 h, Figures 8c, S20 and S21). However, new aggregated forms were only transiently observed but were not anymore detected after 24h. This result was also in accordance with the TEM images where we observed a much less dense network of fibers, although the typical morphology was retained.

**Protection against  $A\beta_{1-42}$  cell toxicity.** The inhibitors were investigated to determine their ability to reduce the toxicity of aggregated  $A\beta_{1-42}$  to SH-SY5Y neuroblastoma cells. The addition of all compounds, to a lesser extent for **G2b**, showed a protective effect on cell survival (MTS assay, Figure 9) and membrane damage (LDH membrane integrity assay, Figure 10) in the presence of cytotoxic 5  $\mu$ M  $A\beta_{1-42}$ . Remarkably, this protective effect was seen at equimolar amounts of inhibitor to  $A\beta_{1-42}$  and was still significant at a very low ratio of 0.1/1 (inhibitor/ $A\beta_{1-42}$ ) in the MTS assay. Both **G2a** and **G1b** showed a slight negative effect on cell viability when incubated with cells alone, although this was negated when  $A\beta$  was present.



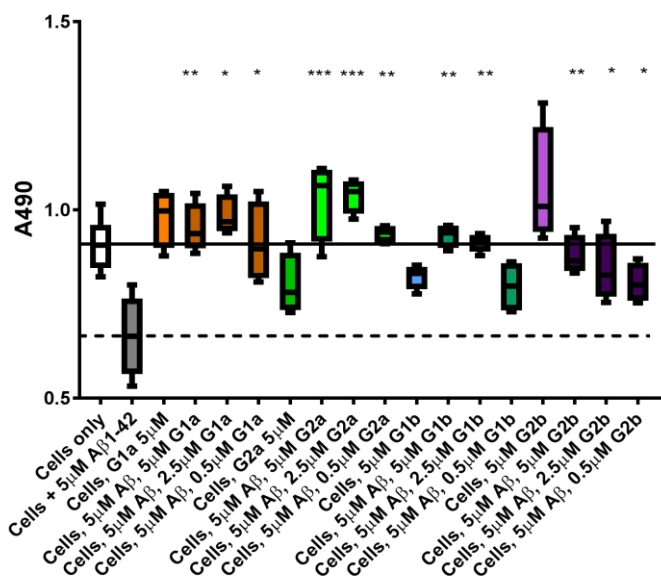


**Figure 9.** Cell viability assay results. The solid line represents the absorbance value seen for cells incubated without  $A\beta_{1-42}$  (white box) and the dotted line that seen for cells incubated with  $5\mu\text{M}$   $A\beta_{1-42}$  (grey box). A statistically significant difference between  $A\beta_{1-42}$  treated cells with and without inhibitor is indicated by \*/\*\*/\*\* corresponding to  $p>0.05/0.01/0.001$ .  $n=4$  for each condition.

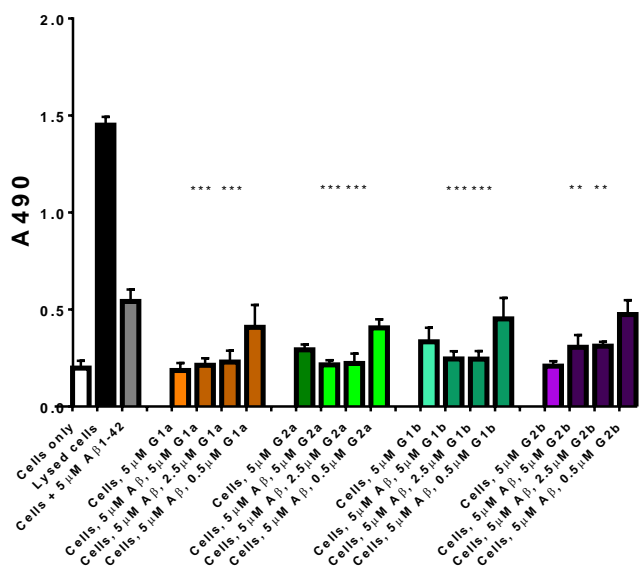


**Figure 10.** LDH based cell toxicity test. Cells were treated in the same manner as with the MTS assay, and cell proliferation was measured using the CytoTox 96<sup>®</sup> NonRadioactive Cytotoxicity Assay Protocol from Promega. Statistical analysis was performed using a student's t test comparing the results for cells exposed to  $5\mu\text{M}$   $A\beta_{1-42}$  with and without inhibitor where \*\* =  $p<0.01$  and \*\*\* =  $p<0.001$ .

This protective effect is more marked than that observed with molecules which have undergone clinical trials<sup>32,33,34</sup> or other molecules recently described as efficient reducers of  $A\beta_{1-42}$  toxicity.<sup>35</sup> In particular, in the literature, resveratrol was reported to protect SH-SY5Y neuroblastoma cells from  $A\beta_{1-42}$  toxicity at 10/1 and 2/1 (resveratrol/ $A\beta_{1-42}$ ) ratios,<sup>32</sup> scyllo-

Inositol was demonstrated to protect PC-12 cells at 10/1 ratio (scyllo-inositol/ $A\beta_{1-42}$ ),<sup>33</sup> and (-)-epigallocatechin-3-gallate (EGCG) protected murine neuro-2a neuroblastoma cells at 1/1 ratio (-)epigallocatechin-3-gallate/ $A\beta_{1-42}$ .<sup>34</sup> In our hands, and comparable to the published data,<sup>32</sup> resveratrol efficiently protected SH-SY5Y neuroblastoma cells only at a ratio of 2/1 (resveratrol/ $A\beta_{1-42}$ ). A stoichiometric ratio 1/1 was less efficient than a substoichiometric ratio of **G1b** and **G2b** (0.5/1 compound/  $A\beta_{1-42}$ ) (Figure 11). Resveratrol exhibits multi-target activity and thus is not selective for  $A\beta_{1-42}$  aggregation. For example, resveratrol inhibits similarly the aggregation of other amyloid proteins such as IAPP<sup>36</sup> (EGCG also inhibits similarly  $A\beta_{1-42}$  and IAPP aggregation in ThT fluorescence assays<sup>37,38</sup>), which is not the case for **G1b** and **G2b**, as mentioned above. By choosing the SREs in our  $\beta$ -hairpin mimics, specifically according to the target amyloid proteins, we can modulate the activity and expect selective activities.

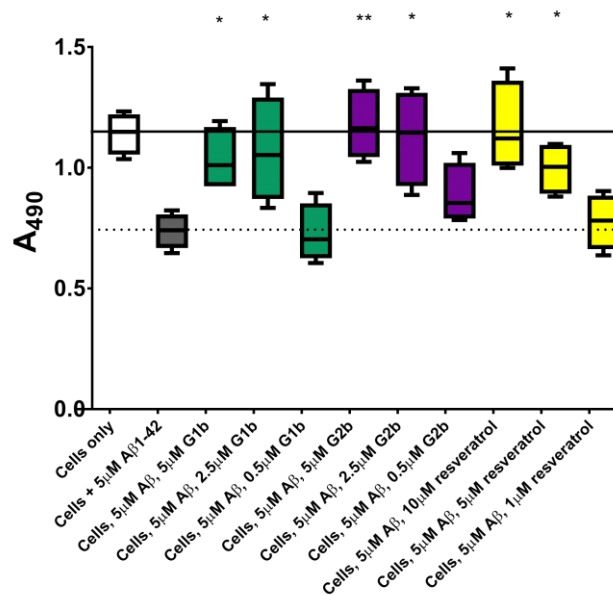


**Figure 11.** Cell viability assay results of resveratrol compared to **G1b** and **G2b**. The solid line represents the mean absorbance value seen for cells incubated without  $A\beta_{1-42}$  (white box) and the dotted line that seen for cells incubated with  $5\mu\text{M}$   $A\beta_{1-42}$  (grey box). A statistically significant difference between  $A\beta_{1-42}$  treated cells with and without inhibitor is indicated by \*/\*\*/\*\* corresponding to  $p>0.05/0.01/0.001$ .  $n=4$  for each condition.

## CONCLUSION

We described new  $\beta$ -hairpin mimics designed on oligomeric and fibril structures of  $A\beta_{1-42}$  and containing a piperidine-pyrrolidine  $\beta$ -turn inducer. The presence of two small recognition sequences able to engage both hydrophobic and ionic interactions with  $A\beta_{1-42}$ , dramatically increased the inhibitory effect on the fibrillization process. Furthermore, the presence of the semi-rigid piperidine-pyrrolidine scaffold **S1** and of the hydrophobic sequence  $G_{33}LMVG_{37}$ , which allows a dynamic equilibrium between different architectures, leads to





the obtainment of compound **G1b** able to inhibit totally the formation of amyloid fibrils. As far as we know, this study is the first example of acyclic small  $\beta$ -hairpin mimics possessing such a highly efficient anti-aggregation activity. This activity is much higher than isolated SREs described in the literature. Furthermore, to the best of our knowledge, this is the first example of compounds able to dramatically preserve the non toxic monomer species of  $A\beta_{1-42}$ . This result might explain the mechanism by which  $\beta$ -hairpin mimics exhibit a strong protective effect on cells even at substoichiometric concentrations. The structural elements made in this study provide valuable insights to explore the design of novel acyclic  $\beta$ -hairpin targeting other types of amyloid-forming proteins.

## Acknowledgements

Géraldine Toutirais (Institut de Biologie Paris Seine (IBPS)/ FR3631, Service de Microscopie Electronique, Université Pierre et Marie Curie, France) is acknowledged for her advice in TEM experiments. The Ministère de l'Enseignement Supérieur et de la Recherche (MESR) and the Alzheimer's Society UK are thanked for financial support for N. Tonali and M. Taylor/D. Allsop respectively. The Laboratory BioCIS is a member of the Laboratory of Excellence LERMIT supported by a Grant from ANR (ANR-10-LABX-33).

## Notes and references

- a) M. Stefani, C. M. Dobson, *J. Mol. Med.*, 2003, **81**, 678–699; b) F. Chiti, C. M. Dobson, *Annu. Rev. Biochem.*, 2006, **75**, 333–366; c) A. Aguzzi, T. O'Connor, *Rev. Drug Discov.*, 2010, **9**, 237–248; d) Y. S. Eisele, C. Monteiro, C. Fearn, S. E. Encalada, R. L. Wiseman, E. T. Powers, J. W. Kelly, *Nat. Rev.*, 2015, **14**, 759–780.
- a) M. Goedert, M. G. A. Spillantini, *Science*, 2006, **314**, 777–780; b) C. Haas, D. J. Selkoe, *Nat. Rev. Mol. Cell. Biol.*, 2007, **8**, 101–112.
- a) F. Belluti, A. Rampa, S. Gobbi, *Exp. Opin. Ther. Pat.*, 2013, **23**, 581–596; b) T. Härd, C. Lendel, *J. Mol. Biol.*, 2012, **421**, 441–465; c) A. J. Doig, P. Derreumaux, *Curr. Opin. Struct. Biol.*, 2015, **30**, 50–56.
- a) J. Mayes, C. Tinker-Mill, O. Kolosov, H. Zhang, B. J. Tabner, D. Allsop, *J. Biol. Chem.*, 2014, **289**, 12052–12062; b) S. I. A. Cohen, S. Linse, L. M. Luheshi, E. Hellstrand, D. A. White, L. Rajah, D. E. Otzen, M. Vendruscolo, C. M. Dobson, T. P. J. Knowles, *Proc. Natl. Acad. Sci. U S A.* 2013, **110**, 9758–9763; c) M. J. Guerrero-Muñoz, D. L. Castillo-Carranza, R. Kayed, *Biochem. Pharm.*, 2014, **88**, 468–478.
- a) C. Haas, D. J. Selkoe, *Nat. Rev. Mol. Cell Biol.*, 2007, 101–112; (b) K. Ono, M. M. Condron, D. B. Teplow, *Proc. Natl. Acad. Sci. U S A.*, 2009, **106**, 14745–14750; (c) P. Prangko, E. C. Yusko, D. Sept, J. Yang, M. Mayer, *PLoS One*, 2012, **7**, e47261; (d) P. Cizas, R. Budvytyte, R. Morkuniene, R. Moldovan, M. Broccio, M. Lösche, G. Niaura, G. Valincius, V. Borutait Arch. *Biochem. Biophys.*, 2010, **496**, 84–92; e) I. Benilova, E. Karran, B. De Strooper *Nat. Neurosci.*, 2012, **15**, 349–357.
- a) P. Vlieghe, V. Lisowski, J. Martinez, M. Khrestchatsky, *Drug Discov. Today*, 2010, **15**, 40–56; (b) F. Albericio, H. G. Kruger, *Future Med. Chem.*, 2012, **4**, 1527–1531; c) T. Uhlig, T. Kyprianou, F. G. Martinelli, C. A. Oppici, D. Heiligers, D. Hills, X. R. Calvo, P. Verhaert, *EuPA Open Proteom.*, 2014, **4**, 58–69.
- a) S. Aileen Funke, D. Willbold *Curr Pharm Des.* 2012, **18**, 755–767; b) M. Chemerovski-Glikman, M. Richman, S. Rahimpour in *Top. Heterocycl. Chem.*, 2016, Publisher: Springer Berlin Heidelberg, 1–32. DOI: 10.1039/C6SC03176E
- a) L. O. Tjénberg, J. Näslund, F. Lindqvist, A. R. Karlström, J. Thyberg, L. Terenius, C. Nordstedt, *J. Biol. Chem.*, 1996, **271**, 8545–8548; b) C. I. Stains, K. Mondal, I. Ghosh, *ChemMedChem*, 2007, **2**, 1674–1692; c) T. Takahashi, H. Mihara, *Acc. Chem. Res.*, 2008, **41**, 1309–1318; d) B. Neddenriep, A. Calciano, D. Conti, E. Sauve, M. Paterson, E. Bruno, D. A. Moffet, *Open Biotechnol. J.*, 2011, **5**, 39–46; e) J. Kumar, R. Namsechi, V. L. Sim, *PLoS One*, 2015, **10**, e0129087; f) V. Parthasarathy, P. L. McClean, C. Hölscher, M. Taylor, C. Tinker, G. Jones, O. Kolosov, E. Salvati, M. Gregori, M. Masserini, D. Allsop, *PLoS One*, 2013; **8**, e54769.
- P.-N. Cheng, C. Liu, M. Zhao, D. Eisenberg, J. S. Nowick, *Nat. Chem.*, 2012, **4**, 927–933.
- a) G. Hopping, J. Kellock, B. Caughey, V. Daggett, *ACS Med. Chem. Lett.*, 2013, **4**, 824–828; b) K. N. L. Huggins, M. Bisaglia, L. Bubacco, M. Tatarek-Nossol, A. Kapurniotu, N. H. Andersen, *Biochemistry*, 2011, **50**, 8202–8212; c) Y. Hamada, N. Miyamoto, Y. Kiso, *Bioorg. Med. Chem. Lett.*, 2015, **25**, 1572–1576.
- a) X. Li, J. Taechalartpaisarn, D. Xin, K. Burgess *Org. Lett.*, 2015, **17**, 632–635; b) E. Ko, A. Raghuraman, L. M. Perez, T. R. Ioerger, K. Burgess *J. Am. Chem. Soc.* 2012, **135**, 167–173.
- a) S. Pellegrino, A. Contini, M. L. Gelmi, L. Lo Presti, R. Soave, E. Erba, *J. Org. Chem.*, 2014, **79**, 3094–3102; b) E. Erba, A. Contini, *RSC Adv.*, 2012, **2**, 10652–10660.
- M. Ahmed, J. David, D. Aucoin, T. Sato, S. Ahuja, S. Aimoto, J. I. Elliott, W. E. Van Nostran, S. O Smith, *Nature Struct. Mol. Biol.*, 2010, **17**, 561–567
- T. Lührs, C. Ritter, M. Adrian, D. Riek-Loher, B. Bohrmann, H. Döbeli, D. Schubert, R. Riek, *Proc. Natl. Acad. Sci. U S A.*, 2005, **102**, 17342–17347.
- K. Hochdörffer, J. März-Berberich, L. Nagel-Steger, M. Epple, W. Meyer-Zaika, A. H. C. Horn, H. Sticht, S. Sinha, G. Bitan, T. Schrader, *J. Am. Chem. Soc.*, 2011, **133**, 4348–4358.
- Y. Sugita, Y. Okamoto, *Chem. Phys. Lett.*, 1999, **314**, 141–151.
- a) F. Ding, D. Tsao, H. Nie, N. V. Dokholyan, *Struct.*, 2008, **16**, 1010–1018; b) E.; Lin, M. S. Shell, *J. Chem. Theory Comput.*, 2009, **5**, 2062–2073; c) P. Tao, J. R. Parquette, C. M. Hadad, *J. Chem. Theory Comput.*, 2012, **8**, 5137–5149.
- a) S. Pellegrino, A. Contini, F. Clerici, A. Gori, D. Nava, M. L. Gelmi *Chemistry- Eur. J.*, 2012, **18**, 8705–8715; b) A. Ruffoni, A. Contini, R. Soave, L. Lo Presti, I. Esposto, I. Maffucci, D. Nava, S. Pellegrino, M. L. Gelmi, F. Clerici, *RSC Adv.*, 2015, 32643–32656; c) I. Maffucci, S. Pellegrino, J. Clayden, A. Contini, *J. Phys. Chem. B*, 2015, **119**, 1350–1361; d) I. Maffucci, J. Clayden, A. Contini, *J. Phys. Chem. B*, 2015, **119**, 14003–14013.
- a) I. Maffucci, A. Contini, *J. Chem. Theor. Comput.*, 2016, **12**, 714–727; b) A. Onufriev, D. Bashford, D. A. Case, *Proteins Struct. Funct. Bioinf.*, 2004, **55**, 383–394.
- W. Kabsch, C. Sander, *Biopol.*, 1983, **22**, 2577–2637.
- a) S. Pellegrino, C. Annoni, A. Contini, F. Clerici, M. L. Gelmi, *Amino Acids*, 2012, **43**, 1995–2003; b) S. Pellegrino, G. Facchetti, A. Contini, M. L. Gelmi, E. Erba, R. Gandolfi, I. Rimoldi, *RSC Adv.*, 2016, **6**, 71529–71533
- P. Cuniasse, I. Raynal, A. Yiiothakis, V. Dive, *J. Am. Chem. Soc.*, 1997, **119**, 5239–5248.
- According to the ref. 12a, in both cases the piperidine scaffold is present as mixture of conformers, making the attribution of piperidine/proline resonances very complicated. As a result, some signals are tentatively assigned.
- a) R. Zerella, *Protein Sciences*, 1999, **8**, 1320–1331; b) L. J. Smith, K. A. Bolin, H. Schwalbe, M. W. Macarthur, J. M. Thornton, C. M. Dobson, *J. Mol. Biol.* 1996, **255**, 494–506.
- L. De Rosa, D. Diana, A. Basile, A. Russomanno, C. Isernia, M. C. Turco, R. Fattorusso, L. D. D'Andrea, *Eur. J. Med. Chem.*, 2014, **73**, 210–216





- 26 a) D. S. Wishart, B. D. Sykes, F. M. Richards, *Biochemistry*, 1992, **31**, 1647-1651; b) D. S. Wishart, C.G. Bigam, A. Holm, R. S. Hodges, B. D. Sykes, *J. Biomol. NMR*, 1995, **5**, 67-81.
- 27 A. M. Fernandez-Escamilla, S. Ventura, L. Serrano, M. A. Nez, *J. Prot. Sci.*, 2006, **15**, 2278-2289.
- 28 H. LeVine, *Methods Enzymol.*, 1999, **309**, 274-284.
- 29 a) M. A. Findeis, G. M. Musso, C. C. Arico-Muendel, H. W. Benjamin, A. M. Hundal, J.-J. Lee, J. Chin, M. Kelley, J. Wakefield, N. J. Hayward, S. M. Molineaux, *Biochemistry*, 1999 **38**, 6791-6800; b) N. Kokkoni, K. Stott, H. Amijee, J. M. Mason, A. J. Doig, *Biochemistry*, 2006 **45**, 9906-9918; c) S. M. Chafekar, H. Malda, M. Merckx, E. W. Meijer, D. Viertl, H. A. Lashuel, F. Baas, W. Scheper, *ChemBioChem*, 2007 **8**, 1857-1864.
- 30 a) M. S. Fernández, *Cell Calcium*, 2014, **56**, 416-427; b) R. Akter, P. Cao, H. Noor, Z. Ridgway, L.-H. Tu, H. Wang, A. G. Wong, X. Zhang, A. Abedini, A. Schmidt, D. P. Raleigh *J. Diabetes Res.*, 2016, Article ID 2798269, 18 pages. doi:10.1155/2016/2798269.
- 31 a) D. Brinet, J. Kaffy, F. Oukacine, S. Glumm, S. Onger, M. Taverna, *Electrophoresis*, 2014, **35**, 3302-3309; b) J. Kaffy, D. Brinet, J.-L. Soulier, I. Correia, N. Tonal, K. F. Fera, Y. Iacone, A. R. F. Hoffmann, L. Khemtemourian, B. Crousse, M. Taylor, D. Allsop, M. Taverna, O. Lequin, S. Onger, *J. Med. Chem.*, 2016, **59**, 2025-2040.
- 32 Y. Feng, X.-P. Wang, S.-G. Yang, Y.-J. Wan, X.-T. Xi, Z. Du, X.-X. Sun, M. Zhao, L. Huang, R.-T. Liu, *Neurotoxicology*, 2009, **30**, 986-995.
- 33 S. Sinha, Z. Du, P. Maiti, F.-G. Klärner, T. Schrader, C. Wang, G. Bitan, *ACS Chem. Neurosci.*, 2012, **3**, 451-458.
- 34 S.-J. Hyunga, A. S. DeTomaa, J. R. Brendera, S. Leec, S. Vivekanandana, A. Kochia, J.-S. Choic, A. Ramamoorthya, B. T. Ruotoloa, M. H. Lima, *Proc. Natl. Acad. Sci. USA.*, 2013, **110**, 3743-3748.
- 35 J. Bieschke, M. Herbst, T. Wiglenda, R. P. Friedrich, A. Boeddrich, F. Schiele, D. Kleckers, J. M. Lopez del Amo, B. A. Grüning, Q. Wang, M. R. Schmidt, R. Lurz, R. Anwyl, S. Schnoeg, M. Fändrich, R. F. Frank, B. Reif, S. Günther, D. M. Walsh, E. E. Wanker, *Nat. Chem. Biol.*, 2012, **8**, 93-101.
- 36 L.-H. Tu, L. M. Young, A. G. Wong, A. E. Ashcroft, S. E. Radford, D. P. Raleigh, *Biochemistry*, 2015, **54**, 666-676.
- 37 F. Meng, A. Abedini, A. Plesner, C. B. Verchere, D. P. Raleigh, *Biochemistry*, 2010, **49**, 8127-8133.
- 38 S. Chan, S. Kantham, V. M. Rao, M. K. Palanivelu, H. L. Pham, P. N. Shaw, R. P. McGeary, B. P. Ross, *Food Chemistry*, 2016, **199**, 185-194.

View Article Online  
DOI: 10.1039/C6SC03176E